

Influence of W, Mo and Ti trace elements on the phase separation in $\text{Al}_8\text{Co}_{17}\text{Cr}_{17}\text{Cu}_8\text{Fe}_{17}\text{Ni}_{33}$ based high entropy alloy



Anna M. Manzoni^{a,*}, Haneen M. Daoud^b, Rainer Voelkl^b, Uwe Glatzel^b, Nelia Wanderka^a

^a Helmholtz-Zentrum Berlin für Materialien und Energie GmbH, Hahn-Meitner-Platz 1, 14109 Berlin, Germany

^b Metals and Alloys, University Bayreuth, Lu dwig-Thoma-Str. 36b, 95447 Bayreuth, Germany

ARTICLE INFO

Article history:

Received 30 August 2014

Received in revised form

2 June 2015

Accepted 9 June 2015

Available online 14 June 2015

Keywords:

High entropy alloys

Atom probe tomography

Transmission electron microscopy

Compositionally complex alloys

ABSTRACT

Compositionally complex alloys, also called high entropy alloys, have been investigated for over a decade in view of different applications, but so far only a small number of alloys can be considered as presenting good enough properties for industrial application. The most common family of elements is Al–Co–Cr–Cu–Fe–Ni. The equiatomic alloy having 5 phases and being too brittle, the composition has been modified in order to improve the mechanical properties. Different compositions have been tested and as a first result ductile $\text{Al}_8\text{Co}_{17}\text{Cr}_{17}\text{Cu}_8\text{Fe}_{17}\text{Ni}_{33}$ has been chosen for deeper investigation. It shows a dendritic segregation into Co–Cr–Fe rich cores and Al–Cu–Ni rich interdendritic sites. The as-cast state is characterized mainly by two phases, namely Al–Cu–Ni rich precipitates of L_{12} structure inside a solid solution matrix. After homogenization both alloys consists of a single solid solution phase. Results are compared to calculations by ThermoCalc. In order to further improve the properties of the alloy the Cr content has been decreased and replaced by trace elements W, Mo and Ti, which, according to ThermoCalc, increase the melting point and the phase transition temperature which leads to the formation of the L_{12} phase. As-cast and heat treated samples of the base and the modified alloy have been investigated by transmission electron microscopy and three dimensional atom probe. Results of the investigations will be discussed in terms of microstructure, hardness and coherence with Thermo Calc predictions.

© 2015 Elsevier B.V. All rights reserved.

1. Introduction

Since their discovery in the beginning of this century [1–4] high entropy alloys, or compositionally complex alloys, have been subject to intensive investigation. However, the initial assumption [1,4], that a mix of five or more elements would lead to a solid solution of all elements because of the high configurational entropy, has been found to be true for only a very small number of alloys. The best known example is the equiatomic CoCrFeMnNi, for which the fcc solid solution can be obtained even in the as-cast state and with a pronounced dendritic morphology [2,5,6]. Another example is the equiatomic MoNbTaVW of bcc structure [7]. Several attempts have been made to find other single phased solid solutions, but there are two main problems: on the one hand there is no universal prediction criterion [8] and on the other hand single phase alloys do not show the best mechanical properties. Thus, a new alloy design concept has been established.

Former works on alloys of the Al–Co–Cr–Cu–Fe–Ni family [9–11] have shown promising results, but the mechanical properties of this

family should be optimized by a choice of the best composition and an adequate heat treatment which lead to a microstructure with good mechanical properties. Equiatomic AlCoCrCuFeNi is a bcc based alloy with five main phases and too brittle for application [10]. Equiatomic AlCoCrFeNi is also bcc based and too brittle, even though it shows only two phases [12]. An improved $\text{Al}_{23}\text{Co}_{15}\text{Cr}_{23}\text{Cu}_8\text{Fe}_{15}\text{Ni}_{16}$ alloy shows three phases, two bcc and one fcc, but it remains too brittle for applications [11]. Finally, after several tests to find a ductile alloy with fcc phases, the $\text{Al}_8\text{Co}_{17}\text{Cr}_{17}\text{Cu}_8\text{Fe}_{17}\text{Ni}_{33}$ alloy has been chosen for further investigation because according to ThermoCalc simulations [13,14] it is supposed to be single phased after homogenization at high temperatures and grow a γ' phase inside a solid solution matrix when annealed at an intermediate temperature. The formation of γ' particles inside a solid solution matrix is known to imply good mechanical properties in Ni-based alloys and this idea is adapted in case of the present high entropy alloys development. The γ' morphology has been observed in the as-cast $\text{Al}_8\text{Co}_{17}\text{Cr}_{17}\text{Cu}_8\text{Fe}_{17}\text{Ni}_{33}$ alloy [11] but the aspect of the γ' precipitates should be improved e.g. by increasing their current size of about 10 nm. This attempt is made by the addition of γ and γ' stabilizers known from Ni-based alloys, namely Mo, Ti and W [15].

* Corresponding author.

E-mail address: anna.manzoni@helmholtz-berlin.de (A.M. Manzoni).

Table 1
Summary of the heat treatments of Alloy A and Alloy B.

State/alloy	Alloy A (Al ₈ Co ₁₇ Cr ₁₇ Cu ₈ Fe ₁₇ Ni ₃₃)	Alloy B (Al ₈ Co ₁₇ Cr ₁₄ Cu ₈ Fe ₁₇ Ni _{34.8} W _{0.1} Mo _{0.1} Ti ₁)
Initial	as-cast	as-cast
Homogenized	1250 °C/1 h	1250 °C/1 h
Homogenized & annealed	1250 °C/1 h + 700 °C/24 h	1250 °C/80 min + 700 °C/24 h
Heat treatments for TAP investigation	700 °C/5 h	1250 °C/80 min + 875 °C/100 h

In addition, trace elements Ti (1 at%), W and Mo (0.1 at% each), have been added with the aim to enlarge the domain of existence of the γ' phase and to increase the melting temperature of the Al₈Co₁₇Cr₁₇Cu₈Fe₁₇Ni₃₃ alloy, which will be called Alloy A. A new alloy with a composition close to Al₈Co₁₇Cr₁₄Cu₈Fe₁₇Ni_{34.8}W_{0.1}Mo_{0.1}Ti₁ was finally made. In the manuscript it will be called Alloy B. ThermoCalc simulations were used for the microstructure development of the alloys in this study. However, the ThermoCalc diagrams show the phase formation in the equilibrium state, and it needs to be checked whether the prediction for the present alloy is valid.

The influence of the addition of W, Mo and Ti to Alloy A on the microstructure formation needs to be clarified. In Ni-based superalloys W and Mo promote the solid solution strengthening of the γ matrix [16]. The partitioning of W to either the γ or the γ' phase in a multicomponent alloy such as Alloy B is hard to predict [17], even though it partitions to γ in basic Ni- superalloys [18]. Mo is expected to partition to the γ phase [18]. Ti is known to partition to the γ' phase and to stabilize its domain of existence. The chemical composition of the phases has often been determined by energy dispersive X-ray (EDX) analysis. However, the partitioning of small amount of elements is difficult to quantify by EDX. One of the methods that allow a quantitative analysis of phases is atom probe tomography (APT).

Thus, in the present study the influence of the small addition of W, Mo and Ti on the microstructure and the phase formation of Alloy B in the as-cast state and after different heat treatments have been investigated by transmission electron microscopy (TEM); the chemical information on the phases has been obtained by atom probe

tomography. The results are compared with those of the base Alloy A. The investigation of the microstructure is accompanied by microhardness measurements in order to understand the influence of the morphological changes on one mechanical property.

2. Experimental

Alloy A was prepared in a vacuum induction furnace of elements with $\geq 99.95\%$ purity. Alloy B was prepared of elements with $\geq 99.999\%$ purity in an induction levitation furnace under argon atmosphere. The alloy was re-melted at least three times in order to ensure homogeneity. At this point the melting temperature of the alloys has been recorded with a pyrometer, which gives only an approximate value of the melting temperature because of its possible error of 50 °C. The ingots solidified in a water cooled Cu crucible into the as-cast state. After different heat treatments the alloys were quenched in water to room temperature. The heat treatments are summarized in Table 1.

Specimens for investigation with optical microscope and scanning electron microscope (Zeiss Ultra) were ground and polished down to a grain size of 50 nm with a final polishing OP-U colloidal silica suspension. Some specimens were etched for 5 s with an etching solution consisting of Mo-acid, HNO₃, HCl and H₂O.

TEM specimens were electropolished with a solution of 83% ethanol, 10% perchloric acid and 7% glycerine at -20 °C and a voltage of 30 V. TEM observations were carried out in a Philips CM30 microscope, operated at 300 kV and equipped with an EDX detector.

Specimens for atom probe investigations were first cut to a size of $0.25 \times 0.25 \times 10$ mm³ and then electropolished in two steps. Final polishing was achieved with a solution of 98 vol% butoxyethanol and 2 vol% perchloric acid at room temperature and a final voltage of 3 V. The tomographic atom probe (CAMECA) used for investigations is operated with a standing DC voltage and 20% pulse fraction, with a pulse repetition rate of 1000 Hz. Investigations are performed at 70 K and in a vacuum better than 10^{-7} Pa.

Vickers microhardness measurements were performed with a load of ~ 0.5 N on a Reichert-Jung MHT-10 microhardness tester.

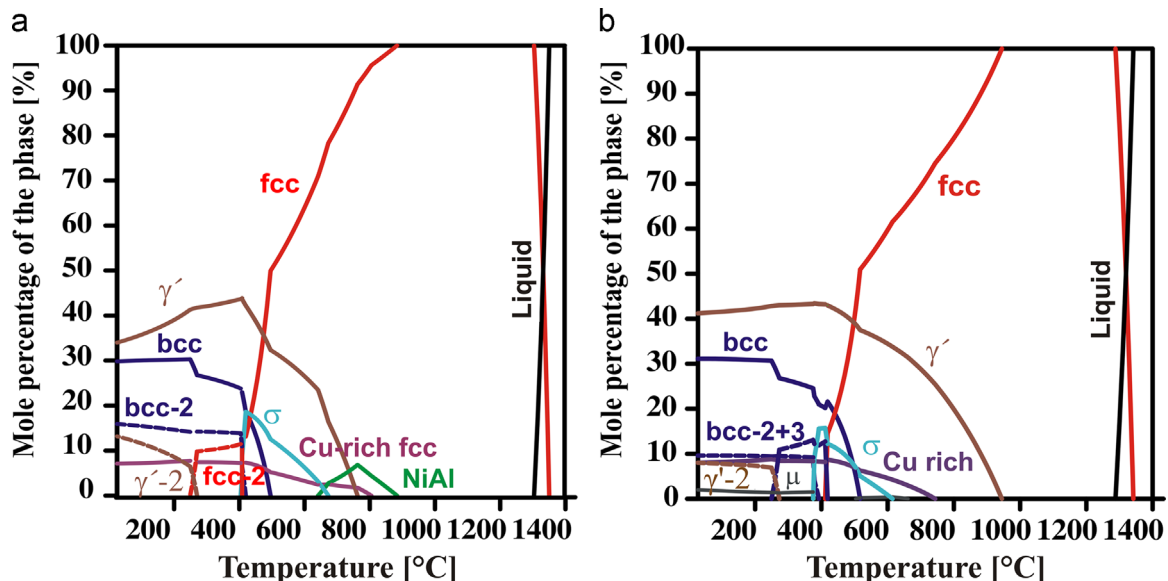


Fig. 1. Phase diagrams calculated by ThermoCalc. (a) Al₈Co₁₇Cr₁₇Cu₈Fe₁₇Ni₃₃ (Alloy A) [11] and (b) Al₈Co₁₇Cr₁₄Cu₈Fe₁₇Ni_{34.8}W_{0.1}Mo_{0.1}Ti₁ (Alloy B). (For interpretation of the references to color in this figure, the reader is referred to the web version of this article.)

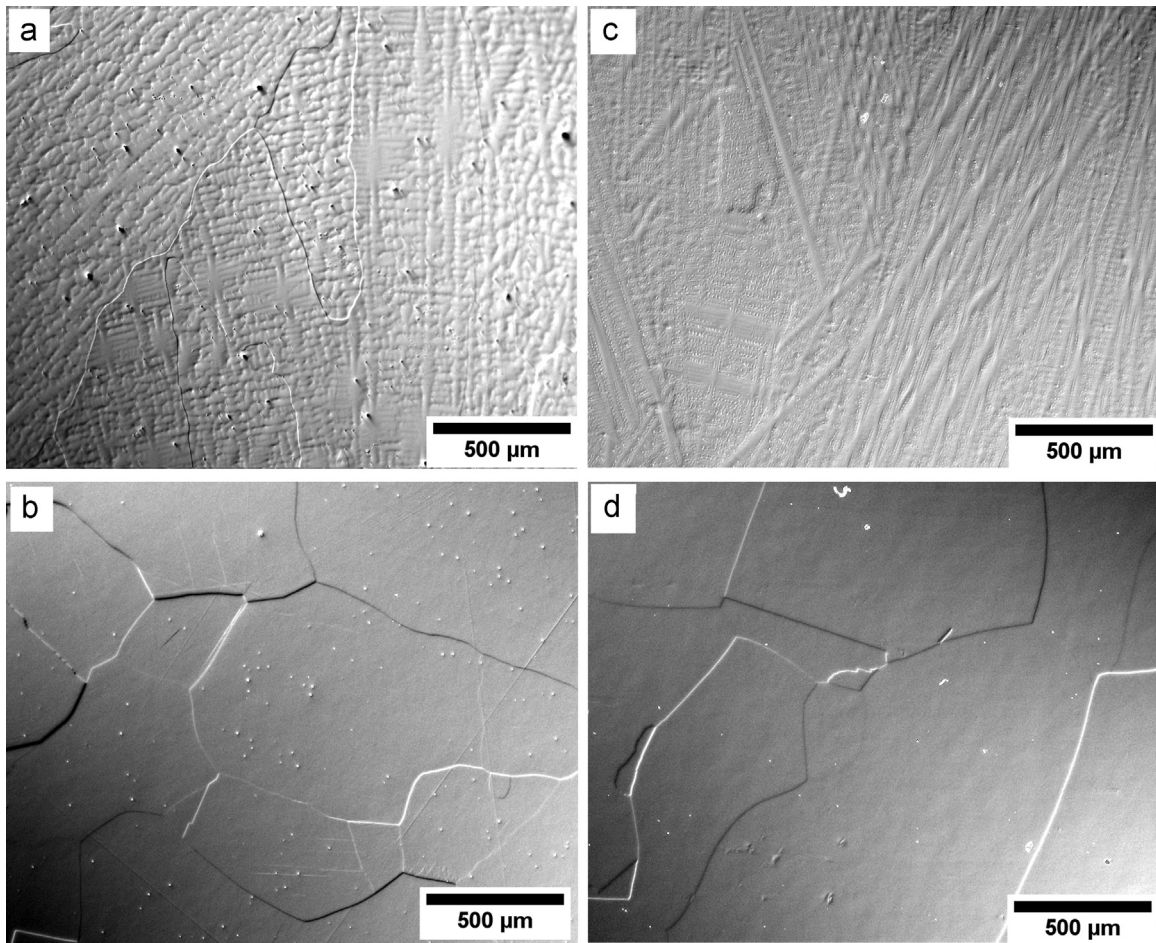


Fig. 2. Optical micrographs of the $\text{Al}_8\text{Co}_{17}\text{Cr}_{17}\text{Cu}_8\text{Fe}_{17}\text{Ni}_{33}$ alloy (Alloy A): (a) as-cast, (b) homogenized at $1250\text{ }^\circ\text{C}/1\text{ h}$; and of the $\text{Al}_8\text{Co}_{17}\text{Cr}_{14}\text{Cu}_8\text{Fe}_{17}\text{Ni}_{34.8}\text{W}_{0.1}\text{Mo}_{0.1}\text{Ti}_1$ alloy (Alloy B): (c) as-cast and (d) homogenized at $1250\text{ }^\circ\text{C}/80\text{ min}$. Dendrites are clearly visible in both non-homogenized samples.

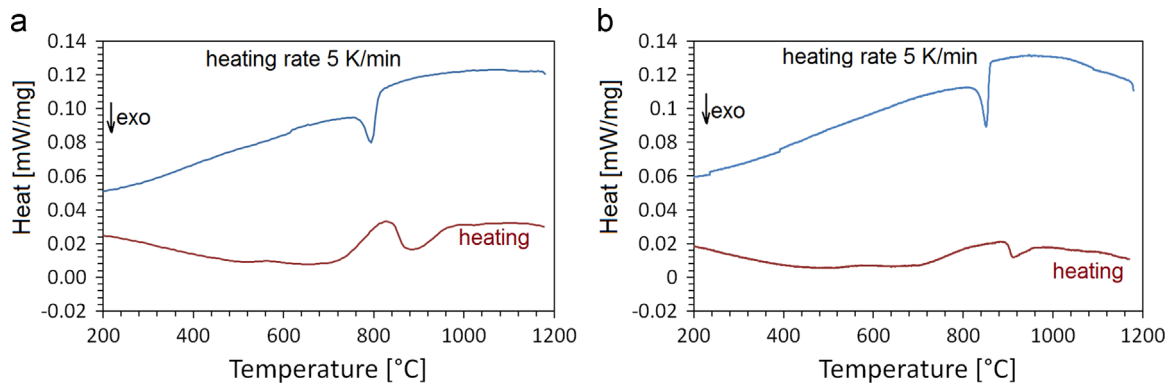


Fig. 3. DSC curves of (a) $\text{Al}_8\text{Co}_{17}\text{Cr}_{17}\text{Cu}_8\text{Fe}_{17}\text{Ni}_{33}$ (Alloy A) and (b) $\text{Al}_8\text{Co}_{17}\text{Cr}_{14}\text{Cu}_8\text{Fe}_{17}\text{Ni}_{34.8}\text{W}_{0.1}\text{Mo}_{0.1}\text{Ti}_1$ (Alloy B). An exothermic peak can be seen in the heating curve at about $840\text{ }^\circ\text{C}$ in the case of Alloy A and at about $920\text{ }^\circ\text{C}$ in the case of Alloy B. These peaks correspond to the γ' formation temperature.

Phase diagrams have been simulated with the CALPHAD-based software ThermoCalc, using the NiT7 database [13,19].

Differential scanning calorimetry (DSC) measurements were carried out in a DSC 404 C Pegasus Thermal analyzer by the Netzsch company and in a DSC by Linseis.

3. Results and discussion

Fig. 1 shows the phase diagrams of both alloys as calculated by ThermoCalc. The already published phase diagram of Alloy A shown in Fig. 1a [11,14] indicates a large number of phases below

$600\text{ }^\circ\text{C}$ which could not be found experimentally. Former studies [11,14] proved the presence of the disordered fcc solid solution matrix marked in red, which is supposed to form above $400\text{ }^\circ\text{C}$, and the γ' phase marked in brown, which is supposed to transform above $\sim 750\text{ }^\circ\text{C}$. At $700\text{ }^\circ\text{C}$, a γ' volume fraction of about 20% is expected. Additionally, Cr carbides have been found in specimens heat treated at $700\text{ }^\circ\text{C}$. The last phase is due to material impurities and could not be predicted by ThermoCalc because impurities have not been taken into account. More details are given in Ref. [14].

The phase diagram in Fig. 1b shows the phases in Alloy B. The evolution of the fcc phase is almost unchanged compared to the

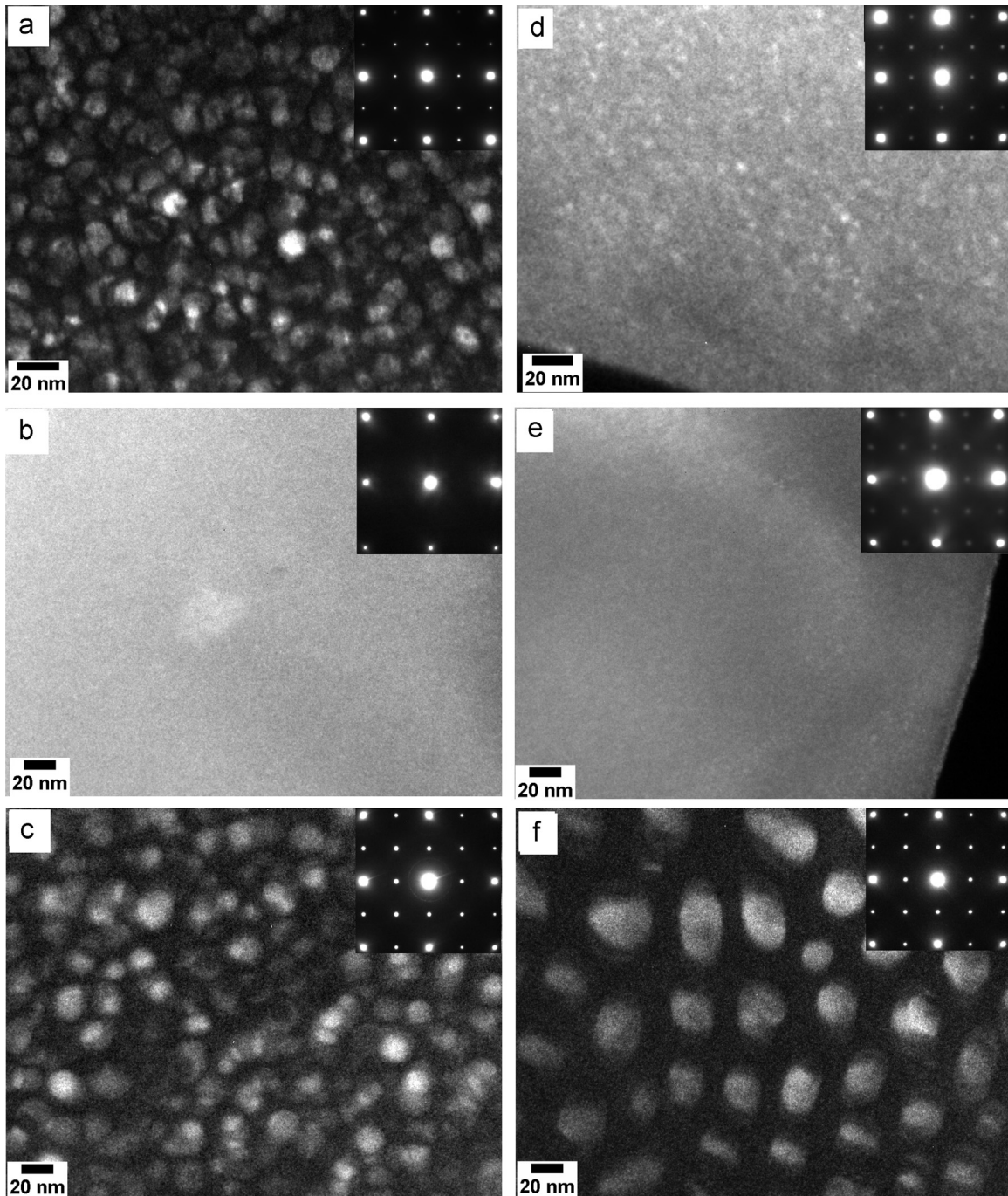


Fig. 4. DF TEM micrographs of the $\text{Al}_8\text{Co}_{17}\text{Cr}_{17}\text{Cu}_8\text{Fe}_{17}\text{Ni}_{33}$ alloy (Alloy A): (a) as-cast, (b) homogenised at $1250\text{ }^\circ\text{C}/1\text{ h}$, (c) annealed at $1250\text{ }^\circ\text{C}/1\text{ h} + 700\text{ }^\circ\text{C}/24\text{ h}$; and of the $\text{Al}_8\text{Co}_{17}\text{Cr}_{14}\text{Cu}_8\text{Fe}_{17}\text{Ni}_{34.8}\text{W}_{0.1}\text{Mo}_{0.1}\text{Ti}_1$ alloy (Alloy B): (d) as-cast, (e) homogenized at $1250\text{ }^\circ\text{C}/80\text{ min}$ and (f) annealed at $1250\text{ }^\circ\text{C}/80\text{ min} + 700\text{ }^\circ\text{C}/24\text{ h}$. The bright imaged Al–Cu–Ni rich precipitates with an L1_2 structure are embedded in the fcc matrix. The corresponding electron diffraction patterns of the [001] zone axis in the insets in (a), (c), (d), (e) and (f) display superlattice reflexions corresponding to the L1_2 structure.

base alloy. The curve of the γ' phase has been shifted upwards and to the right and the phase thus has a higher volume fraction and exists at higher temperatures, as has been expected by the addition of Ti. The NiAl phase predicted in Alloy A has disappeared and thus there is a range of temperature between ~ 730 and $\sim 920\text{ }^\circ\text{C}$ where the desirable morphology (γ' precipitates in solid solution fcc matrix) would exist. At $700\text{ }^\circ\text{C}$ the volume fraction of γ' is expected to be around 35%. The melting temperature according to Fig. 1b has not changed compared to the base alloy (see Fig. 1a). The melting range predicted by ThermoCalc for both alloys lies between 1286 and $1330\text{ }^\circ\text{C}$. The small addition of 1 at% Ti and 0.1 at% of Mo and W does not considerably influence the melting point.

The experimental verification of the ThermoCalc prediction proves difficult for room temperature observations because the cooling of the cast alloys is of course faster than the assumed equilibrium and therefore the formation of phases below $600\text{ }^\circ\text{C}$ is less probable. Thus, the experimental observations of the as-cast alloys are not expected to correspond to the predictions.

The microstructure of the as-cast Alloy A and Alloy B is shown in Fig. 2 using optical microscopy. Two states are being investigated for each alloy, namely the etched as-cast state in (a) and (c) and the one homogenized at $1250\text{ }^\circ\text{C}$ in (b) and (d). The homogenization temperature of $1250\text{ }^\circ\text{C}$ was chosen according to the ThermoCalc diagram, which claims that only one fcc phase for

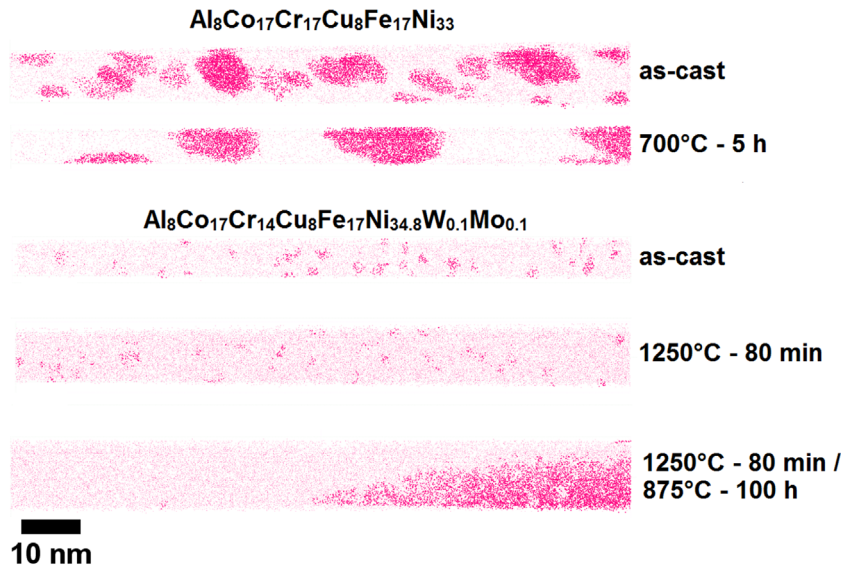


Fig. 5. Three dimensional reconstruction Al atoms (weak dots) positions and Al clusters (big dots) of the $\text{Al}_8\text{Co}_{17}\text{Cr}_{17}\text{Cu}_8\text{Fe}_{17}\text{Ni}_{33}$ alloy (Alloy A) in the as-cast state and heat treated at 700 °C/5 h and of the $\text{Al}_8\text{Co}_{17}\text{Cr}_{14}\text{Cu}_8\text{Fe}_{17}\text{Ni}_{34.8}\text{W}_{0.1}\text{Mo}_{0.1}\text{Ti}_1$ alloy (Alloy B) in the as-cast state, homogenized at 1250 °C/80 min and heat treated at 1250 °C/80 min+875 °C/100 h. Al clusters were analysed using the cluster search module developed by the GPM group in Rouen with a threshold for Al > 15 at% [20].

both alloys is present at this temperature.

The microstructure of the as-cast samples illustrated in Fig. 2 (a) and (c) show a dendritic morphology. Observations with SEM/EDX (not shown here) visualize an enrichment of the high-melting elements Co, Cr and Fe in the dendrite cores and a more (Cu) or less (Al and Ni) pronounced segregation into the interdendritic regions of the low-melting elements Al, Cu and Ni. After the homogenization at 1250 °C dendrites are not visible any more in either alloy. The thermal stability of the investigated alloys was studied by means of DSC in order to determine the temperatures at which heat treatment experiments could be performed to form the γ' phase. The DSC signal of the homogenized samples upon continuous heating at 5 K/min is presented in Fig. 3. An exothermic heat release around 840 °C for Alloy A (a) and around 920 °C for Alloy B (b) can be assigned to the phase formation of the γ' precipitates. The exothermic peak in Fig. 3b is shifted towards higher temperatures after the addition of W, Mo and Ti. The temperature obtained by DSC measurement for Alloy B is in good agreement with the calculated temperature (930 °C) by ThermoCalc, except for a difference of 10 °C. The exothermic peak in Fig. 3a for the Alloy A is much wider than that in Fig. 3b. The difference in the shape can be explained by the fact that, according to the

ThermoCalc diagram, at around 800 °C three different phases are formed and their heat releases interfere with each other. Thus, the difference in temperature between the one calculated (770 °C) by ThermoCalc and the one obtained from DSC (840 °C) is much larger. From these results the temperature of 700 °C was chosen for heat treatment of both alloys to form the γ' phase.

The microstructure is observed after three stages: as-cast, homogenized at 1250 °C and heat treated at 700 °C; and it has been compiled in Fig. 4. Dark field TEM images of Alloy A and Alloy B give a closer view of the inside of the grains (Fig. 4). Fig. 4a shows bright imaged, about 10 nm sized precipitates embedded in a matrix in the as-cast Alloy A. The corresponding SAD confirms that the matrix is a disordered fcc solid solution and the precipitates have an ordered L_{12} structure which is coherent with the matrix. The homogenized Alloy A at 1250 °C/1 h sample in Fig. 4b shows a homogeneous fcc solid solution. No superlattice reflexes can be seen in the corresponding SAD. The same type of precipitates as in the as-cast alloy, though slightly bigger (~20 nm) can be found in the alloy homogenized at 1250 °C/1 h and aged at 700 °C/24 h (Fig. 4c).

Fig. 4d shows the microstructure of the as-cast Alloy B, which is characterized by about 5 nm sized precipitates with L_{12} structure

Table 2

Concentration (in at%) of the phases in Alloy A and Alloy B measured by APT. The error bar corresponds to the standard deviation 2σ . The average cluster size in the homogenized Alloy B is 160 atoms.

	$\text{Al}_8\text{Co}_{17}\text{Cr}_{17}\text{Cu}_8\text{Fe}_{17}\text{Ni}_{33}$ (Alloy A)				$\text{Al}_8\text{Co}_{17}\text{Cr}_{14}\text{Cu}_8\text{Fe}_{17}\text{Ni}_{34.8}\text{W}_{0.1}\text{Mo}_{0.1}\text{Ti}_1$ (Alloy B)					
	As-cast		700 °C/5 h		As-cast		1250 °C/80 min+875 °C/100 h		1250 °C/80 min	
	Matrix	γ' Phase	Matrix	γ' Phase	Matrix	γ' Phase	Matrix	γ' Phase	Matrix	γ' Clusters
Al	6.3 ± 0.3	21.5 ± 1.2	5.1 ± 0.3	22.4 ± 1.7	8.0 ± 0.2	20.6 ± 0.6	7.8 ± 0.4	20.8 ± 0.1	8.7 ± 0.9	18.0 ± 1.6
Co	18.7 ± 0.7	10.0 ± 0.8	19.3 ± 0.5	9.5 ± 0.9	18.9 ± 0.2	13.8 ± 0.6	19.5 ± 0.3	8.8 ± 0.2	17.7 ± 0.6	15.8 ± 0.6
Cr	18.3 ± 0.8	6.5 ± 0.6	19.2 ± 0.2	5.5 ± 1.1	14.3 ± 0.3	8.0 ± 0.3	14.7 ± 0.6	2.6 ± 0.9	13.1 ± 0.1	10.2 ± 0.3
Cu	4.5 ± 0.5	11.7 ± 1.8	4.0 ± 0.8	11.2 ± 1.4	3.3 ± 0.2	4.6 ± 0.3	4.9 ± 0.2	7.4 ± 0.3	5.6 ± 0.6	5.6 ± 0.1
Fe	19.0 ± 0.3	7.1 ± 0.9	19.9 ± 0.8	6.9 ± 1.4	18.0 ± 0.2	11.6 ± 0.8	17.9 ± 0.2	9.5 ± 0.2	17.2 ± 0.6	13.4 ± 0.3
Ni	33.2 ± 1.8	43.3 ± 2.3	32.5 ± 0.3	44.5 ± 1.6	36.3 ± 0.5	39.5 ± 0.8	33.9 ± 0.5	45.3 ± 0.8	36.1 ± 0.6	35.0 ± 0.7
W	–	–	–	–	0.2 ± 0.1	0.2 ± 0.1	0.1 ± 0.1	0.3 ± 0.1	0.2 ± 0.1	0.1 ± 0.1
Mo	–	–	–	–	0.2 ± 0.1	0.2 ± 0.1	0.1 ± 0.1	0.8 ± 0.2	0.2 ± 0.1	0.1 ± 0.2
Ti	–	–	–	–	0.8 ± 0.1	1.7 ± 0.2	0.1 ± 0.0	4.6 ± 0.1	1.2 ± 0.2	1.8 ± 0.1
Vol%	83	17	80	20	85	15	93	7	> 99	< 1

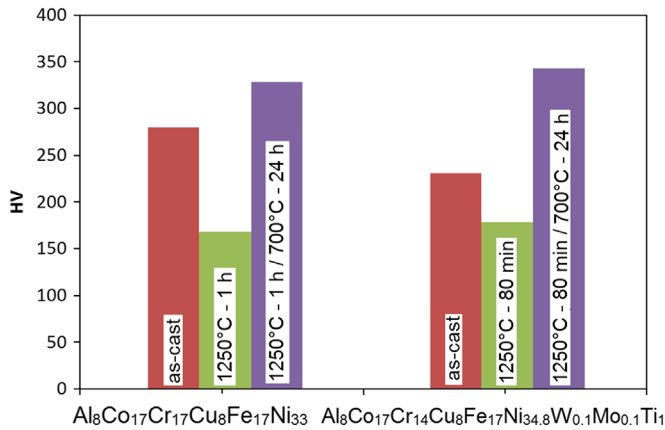


Fig. 6. Evolution of the microhardness of the $\text{Al}_8\text{Co}_{17}\text{Cr}_{17}\text{Cu}_8\text{Fe}_{17}\text{Ni}_{33}$ (Alloy A) and the $\text{Al}_8\text{Co}_{17}\text{Cr}_{14}\text{Cu}_8\text{Fe}_{17}\text{Ni}_{34.8}\text{W}_{0.1}\text{Mo}_{0.1}\text{Ti}_1$ alloy (Alloy B) after different heat treatments.

embedded in the matrix. After homogenization at 1250 °C/80 min small inhomogeneities are obtained and the presence of superlattice spots in the corresponding SAD in Fig. 4e confirm that the homogenization was not completed and some of the coherent L1_2 precipitates remain. The microstructure of sample homogenized at 1250 °C/80 min and subsequently annealed at 700 °C/24 h shows up to 50 nm sized precipitates in Fig. 4f. From this it follows that the addition of W, Mo and Ti leads to an enhanced growth of the γ' phase under the same treatment when compared to the base alloy.

For both alloys the superlattice spots in the SADs are the brightest in the annealed samples. It can thus be assumed that this heat treatment induces the highest ordering.

Complementary to TEM investigations the APT technique has been applied for a quantitative determination of the phase compositions, particularly for very fine precipitates at which individual atoms are resolved.

Fig. 5 shows the three dimensional reconstruction of Al of the specimens investigated by APT. Al has been chosen because of its sharpest transition from the matrix to the precipitates. The reconstruction of all other elements has been omitted for the sake of clarity. The weak dots correspond to all Al atoms. The big dots belong to the Al clusters, which have been calculated with the cluster search module developed by the GPM group in Rouen [20]. They have been calculated with a threshold of 15 at% Al.

The APT reconstructions of Alloy A show about 10 nm (as-cast) and 20 nm (700 °C/ 5 h) sized Al rich phases, which correspond to the Al–Cu–Ni rich γ' phase with L1_2 structure. The APT reconstructions of the Alloy B shows very small Al rich clusters both in the as-cast state and after the heat treatment at 1250 °C/80 min. In the latter the Al rich clusters are extremely small (~ 2 nm) and their volume fraction is negligible (see Table 2). The heat treated specimen at 1250 °C/80 min + 875 °C/100 h shows a region where the matrix meets an Al–Cu–Ni rich γ' precipitate. The measurements confirm the observations made by TEM and allow the determination of the composition in the precipitates. All concentrations and volume fractions as calculated with the lever rule diagram [21] are summarized in Table 2.

APT investigations of Alloy B clearly identify in the mass spectrum but their partitioning to one phase or the other cannot really be determined. However, Ti is found to partition into the γ' phase, as can be seen in the as-cast specimen and in the heat treated at 1250 °C/80 min + 875 °C/100 h. The partitioning of Ti towards the γ' phase corresponds to what has been expected.

Since the mechanical properties are correlated with the microstructure, the microhardness has been measured on samples of the states shown in Fig. 4. Fig. 6 shows the Vickers microhardness

measurements of both alloys at three different states. The addition of W, Mo and Ti softens the alloy in the as-cast state. This can be explained by the smaller size of the Al–Cu–Ni rich γ' precipitates, as can be seen in Fig. 4a and d. APT measurements also show that the volume fraction of the γ' precipitates is lower in the Alloy B alloy ($\sim 15\%$) than in the Alloy A ($\sim 20\%$). In both alloys the specimens heat treated at 1250 °C are the softest. However, in the homogenized state the Alloy B is slightly harder because of the presence of some γ' precipitates that have not been removed by the homogenization treatment (see Fig. 5). The heat treatment at 1250 °C/1 h + 700 °C/24 h induces the highest hardness in both alloys. This subsequent annealing at 700 °C/24 h makes the Alloy B harder than the Alloy A because the average size of the γ' precipitates in the former is bigger than in the latter. The tendency in the microhardness is in accordance with observations in Ni base alloys, in which the best mechanical properties are obtained for precipitates of about 500 nm in size [22]. In our study the size of the γ' precipitates is far away from this optimum. To find the right heat treatment in order to produce large γ' precipitates is the next step of our investigations. In addition, the mechanical properties of Ni-based alloys are derived from the volume fraction of γ' precipitates which nowadays reaches 70–80% [15]. To reach the maximum volume fraction of γ' precipitates in the alloy with additions of W, Mo and Ti is another aim for the future investigations.

It can thus be concluded that the controlled formation of ordered precipitates enhances the hardness and the initial concept of high entropy alloys concerning the benefits of a solid solution does not apply. The addition of γ' stabilizers shows this even more clearly.

4. Conclusions

Experimental results obtained by TEM and APT and calculations with ThermoCalc have enlightened the influence of the small additions of W, Mo and Ti to the microstructure of the $\text{Al}_8\text{Co}_{17}\text{Cr}_{17}\text{Cu}_8\text{Fe}_{17}\text{Ni}_{33}$ alloy. The following insights have been obtained:

- Ti was found preferentially in the γ' precipitates, as expected from Ni based superalloys.
- No preferential partitioning has been found for either W nor Mo. They are equally distributed in both the γ' and the γ phase.
- Another important aspect is that the addition of W, Mo and Ti leads to the enlargement of the existence region of the γ' phase.
- The controlled formation of ordered particles inside a solid solution matrix enhances the microhardness of the alloy.
- The prediction of the phase formation by ThermoCalc simulation is valid for the high temperature region.

The modification of the $\text{Al}_8\text{Co}_{17}\text{Cr}_{17}\text{Cu}_8\text{Fe}_{17}\text{Ni}_{33}$ alloy by W, Mo and Ti additions was found to be an effective approach to stabilize and to improve the microstructure with respect to high temperature applications.

Acknowledgements

The authors are grateful to the German Research foundation (DFG) for the financial support by WA 1378/15-2 and GL 181/25-2. The authors would like to thank C. Förster and C. Leistner for sample preparation.

References

- [1] J.W. Yeh, Nano-structured high-entropy alloys, *Knowl. Bridge* 40 (2003) 1–2.
- [2] B. Cantor, I.T.H. Chang, P. Knight, A.J.B. Vincent, Microstructural development in equiatomic multicomponent alloys, *Mater. Sci. Eng. A* 375 (2004) 213–218.
- [3] S. Ranganathan, Alloyed pleasures: multimetallic cocktails, *Curr. Sci.* 85 (2003) 1404–1406.
- [4] J.W. Yeh, S.K. Chen, S.J. Lin, J.Y. Gan, T.S. Chin, T.T. Shun, C.H. Tsau, S.Y. Chang, Nanostructured high-entropy alloys with multiple principal elements: novel alloy design concepts and outcomes, *Adv. Eng. Mater.* 6 (2004) 299–303.
- [5] B. Ren, Z.X. Liu, D.M. Li, L. Shi, B. Cai, M.X. Wang, Effect of elemental interaction on microstructure of CuCrFeNiMn high entropy alloy system, *J. Alloy. Compd.* 493 (2010) 148–153.
- [6] K.Y. Tsai, M.H. Tsai, J.W. Yeh, Sluggish diffusion in Co–Cr–Fe–Mn–Ni high-entropy alloys, *Acta. Mater.* 61 (2013) 4887–4897.
- [7] O.N. Senkov, G.B. Wilks, D.B. Miracle, C.P. Chuang, P.K. Liaw, Refractory high-entropy alloys, *Intermetallics* 18 (2010) 1758–1765.
- [8] S. Praveen, B.S. Murty, R.S. Kottada, Alloying behavior in multi-component AlCoCrCuFe and NiCoCrCuFe high entropy alloys, *Mater. Sci. Eng. A* 534 (2012) 83–89.
- [9] S. Singh, N. Wanderka, K. Kiefer, K. Siemensmeyer, J. Banhart, Effect of de-composition of the Cr–Fe–Co rich phase of AlCoCrCuFeNi high entropy alloy on magnetic properties, *Ultramicroscopy* 111 (2011) 619–622.
- [10] S. Singh, N. Wanderka, B.S. Murty, U. Glatzel, J. Banhart, Decomposition in multi-component AlCoCrCuFeNi high-entropy alloy, *Acta. Mater.* 59 (2011) 182–190.
- [11] A. Manzoni, H. Daoud, S. Mondal, S. van Smaalen, R. Völkl, U. Glatzel, N. Wanderka, Investigation of phases in Al₂₃Co₁₅Cr₂₃Cu₈Fe₁₅Ni₁₆ and Al₈Co₁₇Cr₁₇Cu₈Fe₁₇Ni₃₃ high entropy alloys and comparison with equilibrium phases predicted by Thermo-Calc, *J. Alloy. Compd.* 552 (2013) 430–436.
- [12] A. Manzoni, H. Daoud, R. Völkl, U. Glatzel, N. Wanderka, Phase separation in equiatomic AlCoCrFeNi high-entropy alloy, *Ultramicroscopy* 132 (2013) 212–215.
- [13] Thermotech Ni-based Superalloys Database, TTNi7, Thermo-Calc Software AB, Stockholm, Sweden, 2006.
- [14] H.M. Daoud, A. Manzoni, R. Völkl, N. Wanderka, U. Glatzel, Microstructure and tensile behavior of Al₈Co₁₇Cr₁₇Cu₈Fe₁₇Ni₃₃ (at%) high-entropy alloy, *JOM* 65 (2013) 1805–1814.
- [15] R.C. Reed, *The Superalloys: Fundamentals and Applications*, Cambridge University Press, Cambridge, 2006.
- [16] D. Blavette, E. Cadel, C. Pareige, B. Deconihout, P. Caron, Phase transformation and segregation to lattice defects in Ni-base superalloys, *Microsc. Microanal.* 13 (2007) 464–483.
- [17] Y. Amouyal, Z.G. Mao, D.N. Seidman, Effects of tantalum on the partitioning of tungsten between the γ and γ' -phases in nickel-based superalloys: linking experimental and computational approaches, *Acta. Mater.* 58 (2010) 5898–5911.
- [18] M. Durand-Charre, *The Microstructure of Superalloys*, CRC Press, Boca Raton, London, New York, Washington D.C., 1997.
- [19] The Version TCCR, ThermoCalc Software AB, Stockholm, Sweden, 2006. (<http://www.thermocalc.com>).
- [20] X. Sauvage, G. Da Costa, R.Z. Valiev, 3D atom probe investigation of cementite dissolution in a pearlitic steel processed by high pressure torsion, in: Y.T. Zhu, T.G. Langdon, T.G. Valiev, S.L. Semiatin, D.H. Shin, T.C. Lowe (Eds.), *Ultrafine Grained Materials III*, TMS, Warrendale, PA, 2004, pp. 31–36.
- [21] D. Blavette, P. Caron, T. Khan, An atom probe investigation of the role of rhenium additions in improving creep resistance of Ni-base superalloys, *Scr. Metall.* 20 (1986) 1395–1400.
- [22] E. Fleischmann, C. Konrad, J. Preussner, R. Völkl, E. Affeldt, U. Glatzel, Influence of solid solution hardening on creep properties of single-crystal nickel-based superalloys, *Metall. Mater. Trans. A-Phys. Metall. Mater. Sci.* 46A (2015) 1125–1130.